

Supplementary Information

**Solid-state and liquid-free elastomeric ionic conductors
with autonomous self-healing ability†**

Xinxin Qu, Wenwen Niu, Rui Wang, Zequan Li, Yue Guo, Xiaokong Liu* and Junqi Sun

State Key Laboratory of Supramolecular Structure and Materials, College of Chemistry, Jilin University, Changchun 130012, P. R. China. Email: xiaokongliu@jlu.edu.cn

Supplementary figures and tables: Fig. S1-Fig. S13, Table S1-Table S3

Supplementary references

Supplementary movie: Movie S1

Supplementary figures and tables

Table S1. Summary of the molecular weights (M_n and M_w) of the different PIL/AcO copolymers.

PIL/AcO copolymers	M_n	M_w
PIL-1/AcO	11144	14958
PIL-2/AcO	11816	16194
PIL-3/AcO	13794	22693

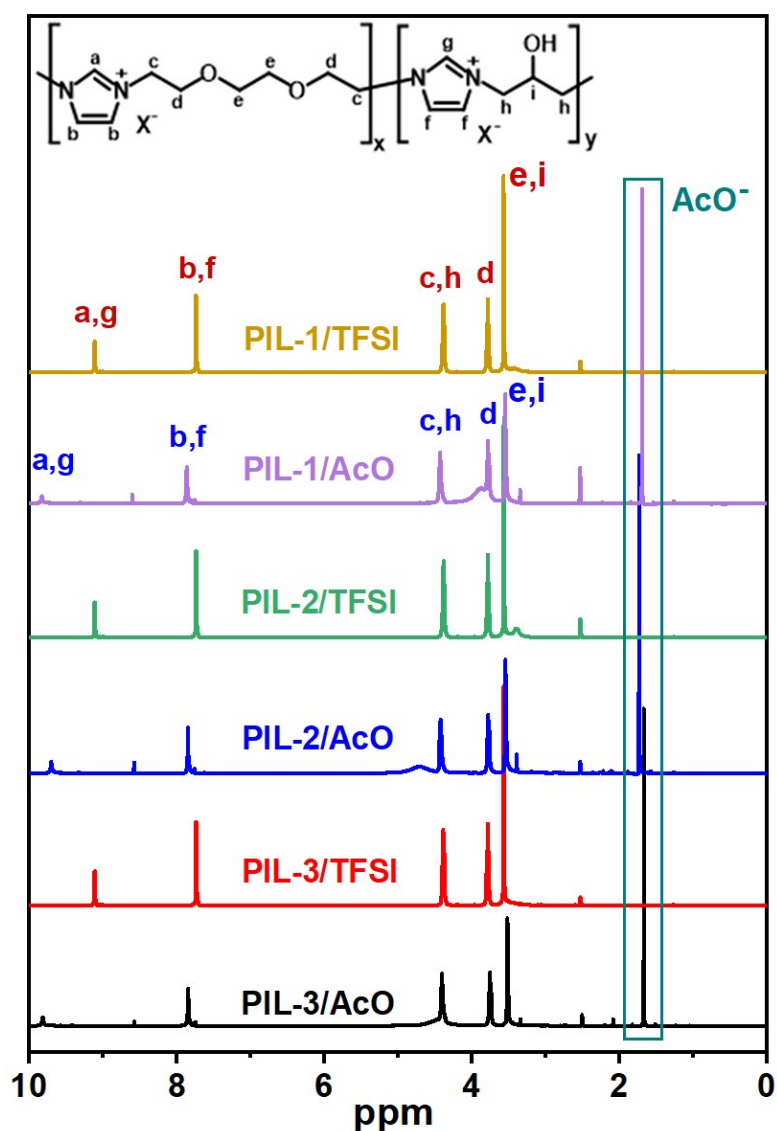


Fig. S1 ^1H NMR (DMSO- d_6 , 500 MHz) spectra of the PIL/AcO and PIL/TFSI copolymers.

In the ^1H NMR spectra of the PIL/AcO copolymers, the peaks at δ 1.70 ppm are assigned to the protons from the AcO^- anions. After the anion exchange from AcO^- into TFSI $^-$, the peaks assigned to the AcO^- anions completely disappear and the C2-proton peaks (a,g) of the imidazolium cation shift to lower chemical shifts, in the PIL/TFSI copolymers. These results confirm the successful substitution of TFSI $^-$ for AcO^- .

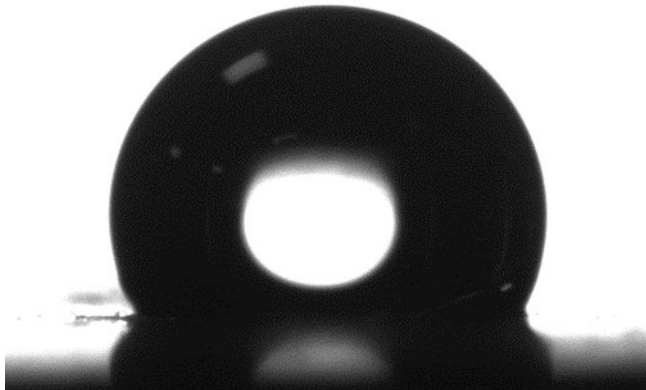


Fig. S2 Water contact angle on the surface of the PIL-2/TFSI elastomer.

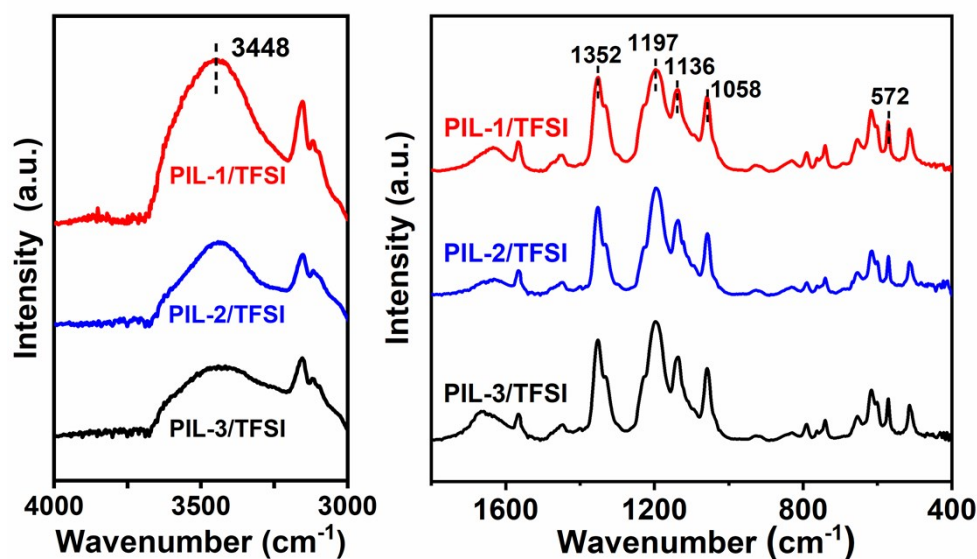


Fig. S3 FTIR spectra of the PIL/TFSI copolymers.

The FTIR absorption band at 1136 cm^{-1} is assigned to the C-O-C groups from the IL-EO units, while the absorption bands at 1352 , 1197 , 1058 and 572 cm^{-1} are assigned to the TFSI⁻ ions. The broad absorption bands of the hydroxyl groups center at 3448 cm^{-1} , suggesting that the hydroxyl groups are hydrogen-bonded.^{S1,S2}

Supplementary references

S1 L. J. Bellamy, *The Infra-red Spectra of Complex Molecules*. John Wiley: New York, 1975.

S2 T. KONDO, *Cellulose*, 1997, 4, 281-292.

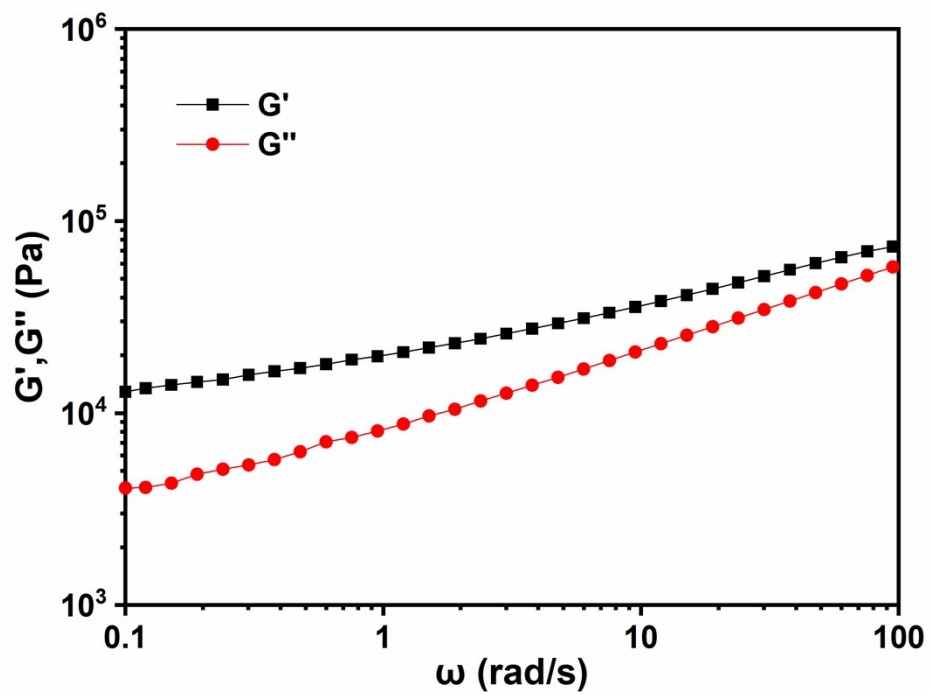


Fig. S4 Storage modulus (G') and loss modulus (G'') of the PIL-2/TFSI elastomer as a function of the oscillation frequency.

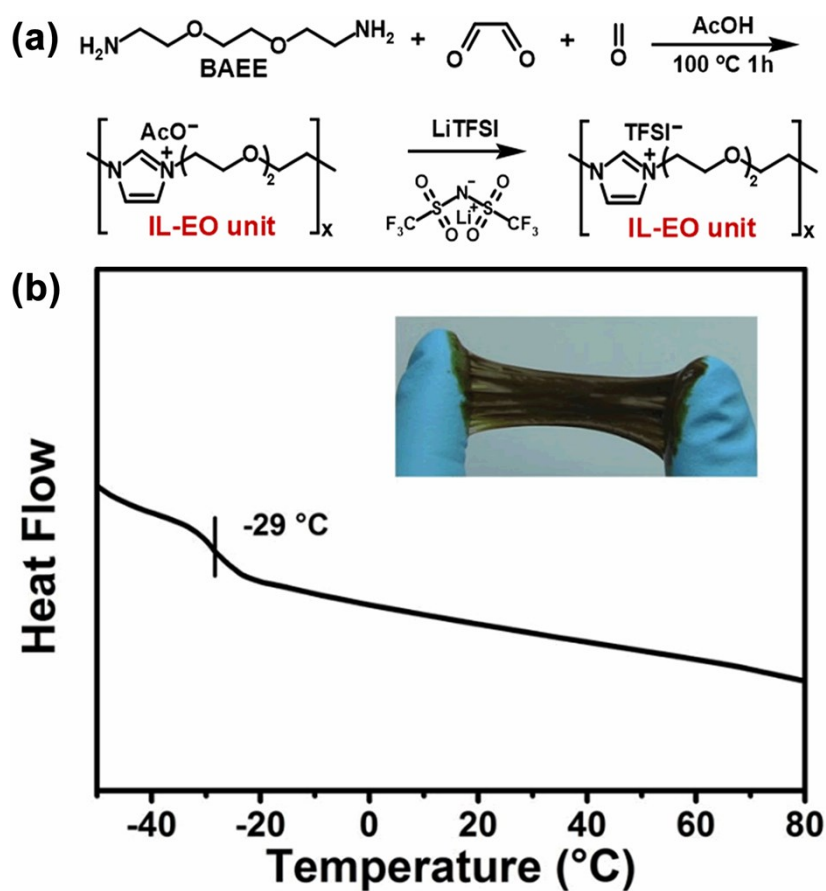


Fig. S5 (a) Schematic illustration of the synthetic procedure of the PIL/TFSI homopolymer that comprises only the IL-EO units. (b) DSC spectrum and photograph (inset) of the PIL/TFSI homopolymer.

Table S2 Summary of the mechanical properties of the different PIL/TFSI elastomers, measured at the stretching speed of 50 mm/min.

PIL/TFSI copolymers	Tensile strength (MPa)	Young's modulus (MPa)	Elongation-at-break (%)	Toughness (MJ/m ³)
PIL-1/TFSI	0.40 ± 0.08	0.18 ± 0.01	320 ± 60	0.62 ± 0.02
PIL-2/TFSI	0.24 ± 0.04	0.071 ± 0.004	540 ± 50	0.61 ± 0.06
PIL-3/TFSI	0.14 ± 0.02	0.024 ± 0.003	980 ± 130	0.64 ± 0.02

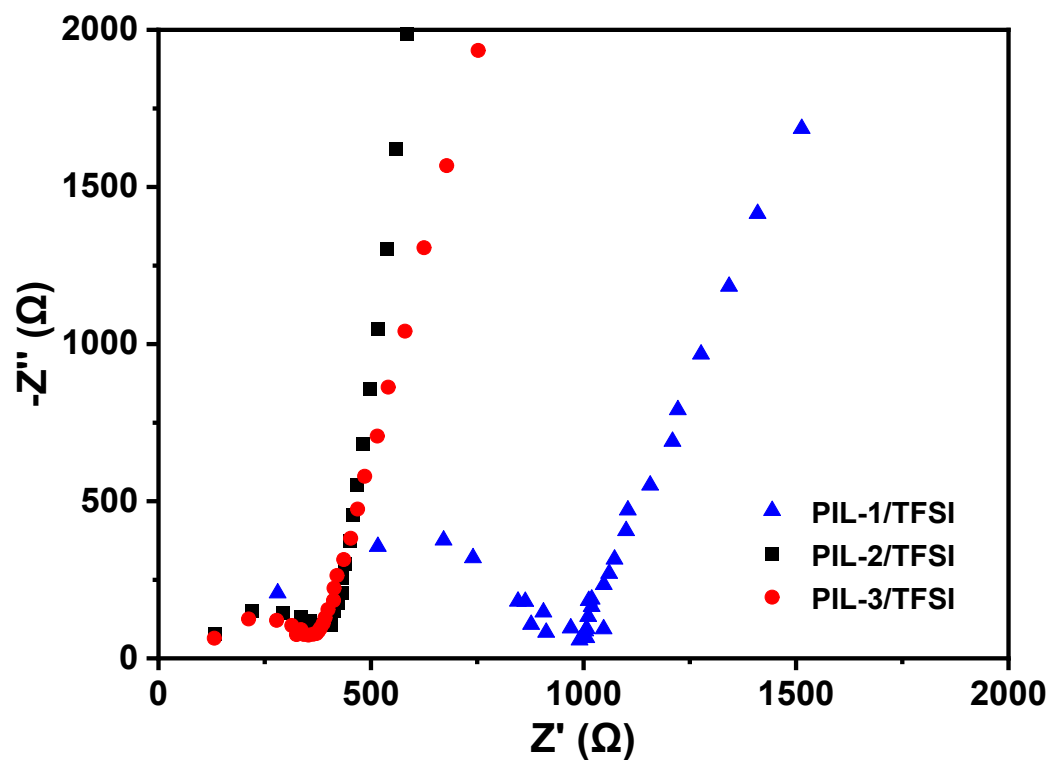


Fig. S6 Nyquist plots of impedance spectra of the different PIL/TFSI elastomers, which were measured by the electrochemical workstation and used for the determination of the ionic conductivity of the samples.

Table S3 Comparison of the ionic conductivity, tensile strength and elongation-at-break between the solid-state and liquid-free PIL-2/TFSI elastomer and some of the previously reported stretchable ionic conductors.

<i>Materials</i>	σ at RT [$mS\ cm^{-1}$]*	σ_b [MPa]*	ϵ [%]*	<i>Reference</i>
Self-healing, solid-state and liquid-free PIL-2/TFSI elastomer	0.131 ± 0.01	0.24 ± 0.04	540 ± 50	This work
Ion-conductive elastomer involving liquid plasticizer	0.12	2.5 ± 0.12	1870 ± 110	S3
Ion-conductive elastomer involving liquid plasticizer	0.25	ca. 0.45	ca. 135	S4
Ionogel (P(VDF-HFP) + ionic liquids)	1.05×10^{-2}	ca. 0.08	ca. 2000	S5
Ionogel (polymer network + deep eutectic solvents)	0.4	ca. 0.3	ca. 450	S6
Ionogel (polymer network + deep eutectic solvents)	0.014-0.028	0.047-0.152	723-1092	S7
Liquid-free ion-conductive elastomer	1.27×10^{-4}	ca. 0.24	ca. 1100	S8
Liquid-free ion-conductive elastomer	5.7×10^{-4} - 2.4×10^{-3}	0.09-0.11	120-140	S9

* σ at RT, σ_b and ϵ represent ionic conductivity at room temperature, tensile strength and elongation-at-break, respectively.

Supplementary references

- S3 D. G. Mackanic, X. Yan, Q. Zhang, N. Matsuhisa, Z. Yu, Y. Jiang, T. Manika, J. Lopez, H. Yan, K. Liu, X. Chen, Y. Cui and Z. Bao, *Nat. Commun.*, 2019, **10**, 5384.
- S4 J. Lopez, Y. Sun, D. G. Mackanic, M. Lee, A. M. Foudeh, M.-S. Song, Y. Cui and Z. Bao, *Adv. Mater.*, 2018, **30**, 1804142.
- S5 Y. Cao, Y. J. Tan, S. Li, W. W. Lee, H. Guo, Y. Cai, C. Wang and B. C. K. Tee, *Nat. Electron.*, 2019, **2**, 75-82.
- S6 R. Li, T. Fan, G. Chen, K. Zhang, B. Su, J. Tian and M. He, *Chem. Mater.*, 2020, **32**, 874-881.
- S7 C. Dang, M. Wang, J. Yu, Y. Chen, S. Zhou, X. Feng, D. Liu and H. Qi, *Adv. Funct. Mater.*, 2019, **29**, 1902467.
- S8 L. Shi, T. Zhu, G. Gao, X. Zhang, W. Wei, W. Liu and S. Ding, *Nat. Commun.*, 2018, **9**, 2630.

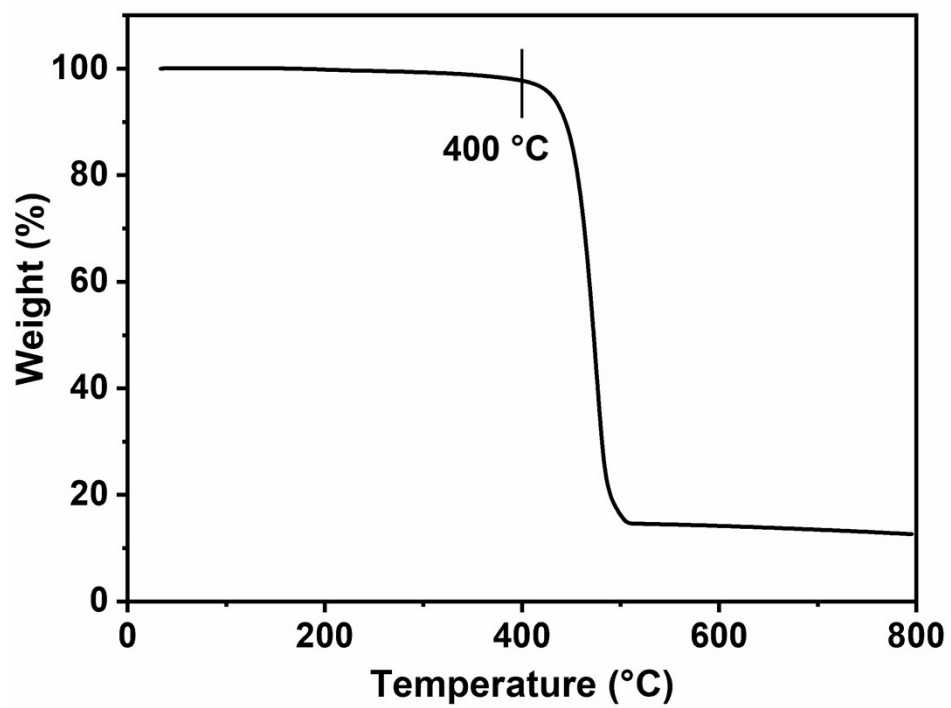


Fig. S7 TGA curve of the PIL-2/TFSI elastomer.

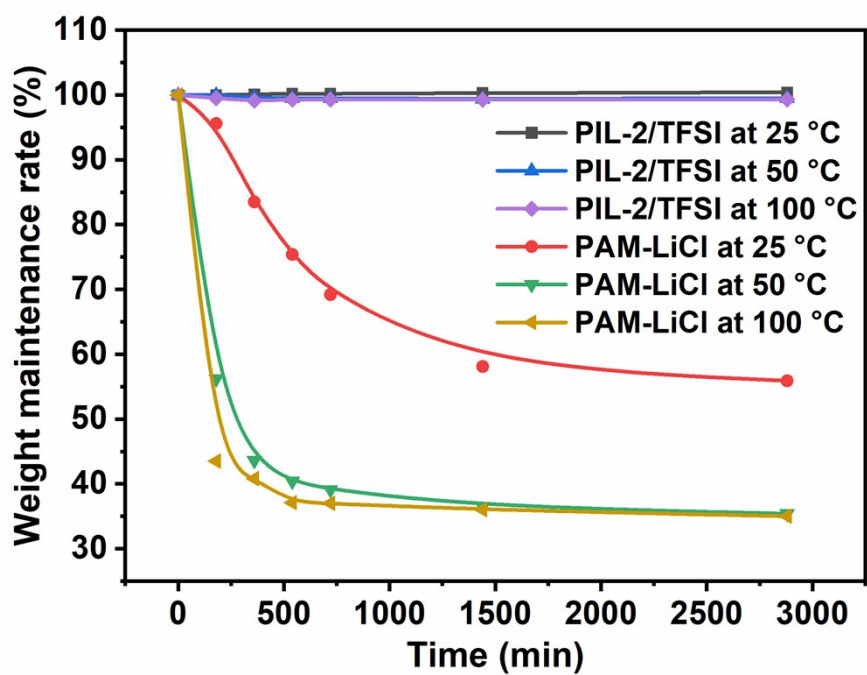


Fig. S8 Time-dependent evolution of weights of the PIL-2/TFSI elastomers and PAM-LiCl hydrogels, which were incubated in the open air at different temperatures.

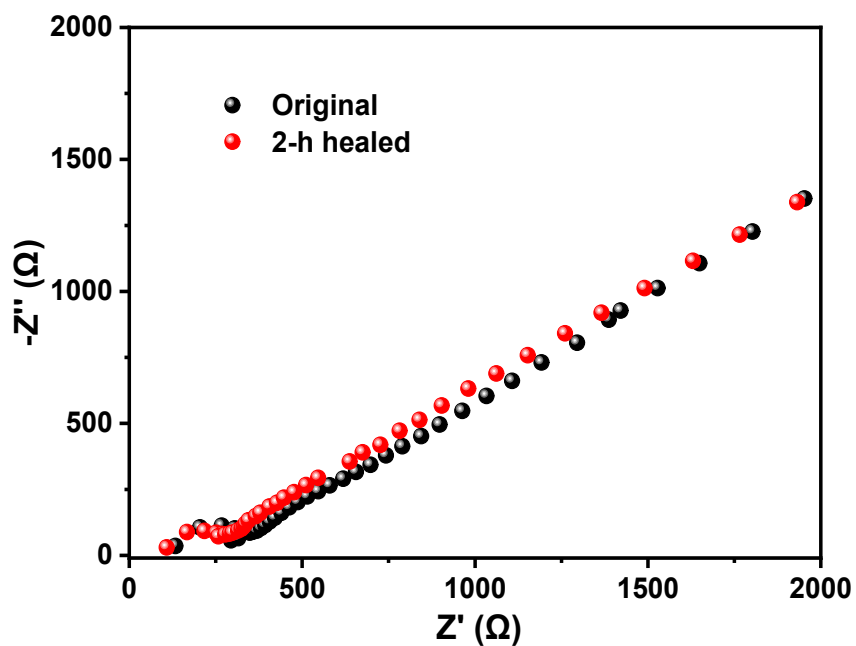


Fig. S9 Nyquist plots of impedance spectra of the original and 2-h healed PIL-2/TFPI elastomer that was previously cut into two separate pieces. The impedance spectra were measured by the electrochemical workstation and used for the determination of the ionic conductivity of the samples.

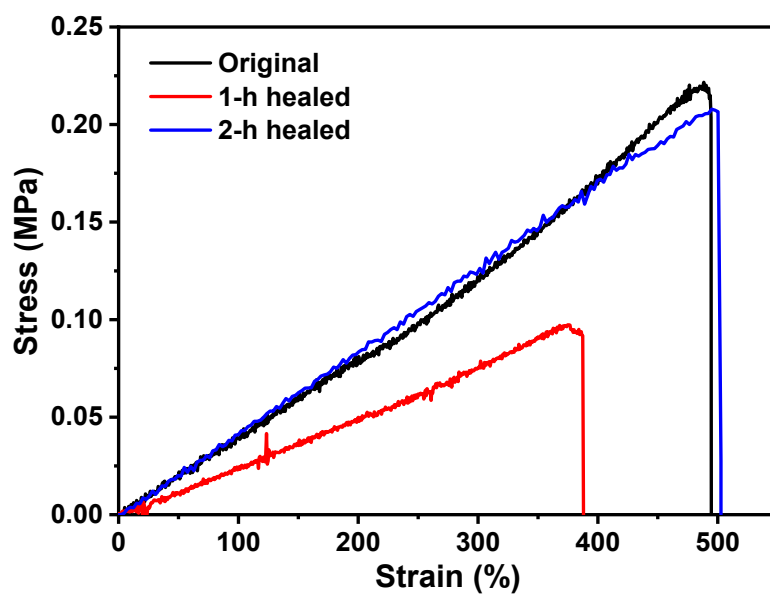


Fig. S10 Stress-strain curves of the original, 1-h and 2-h healed PIL-2/TFSI elastomers. The 1-h and 2-h healed elastomers were previously cut into two separate pieces. The healing process was conducted in the relative humidity of 100% at room temperature.

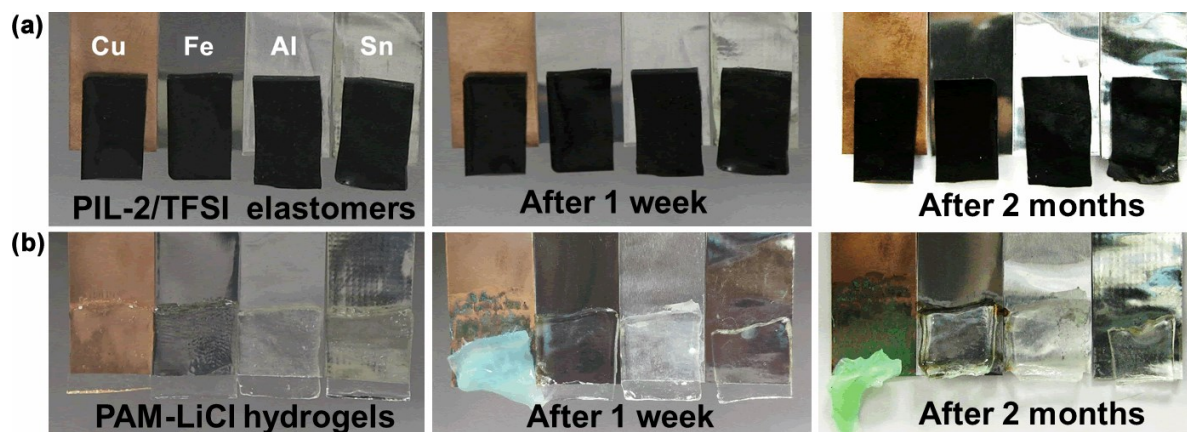


Fig. S11 (a,b) Photographs of the PIL-2/TFSI elastomers (a) and PAM-LiCl hydrogels (b), adhered to different metal substrates (Cu, Fe, Al and Sn), after being placed in the open air (a) and in a sealed box (b), respectively, for different times.

Due to the dry nature of the PIL-2/TFSI elastomer, the elastomer-metal joints exhibit long-term stability because there are minimal reactions between the elastomer and metals in air. As shown in Fig. S11a, the appearances of the elastomers adhered to the metals show little change and no corrosion of the metals was observed after 2-month incubation in the open air, though some of the metals are slightly oxidized by air. In contrast, the PAM-LiCl hydrogel-metal joints undergo obvious degradation even that they were placed in a sealed box (Fig. S11b). The hydrogels show obvious shrinkage after 2-month incubation in a sealed box due to the evaporation of water, and the hydrogels cause severe corrosion to the metals (Fig. S11b).

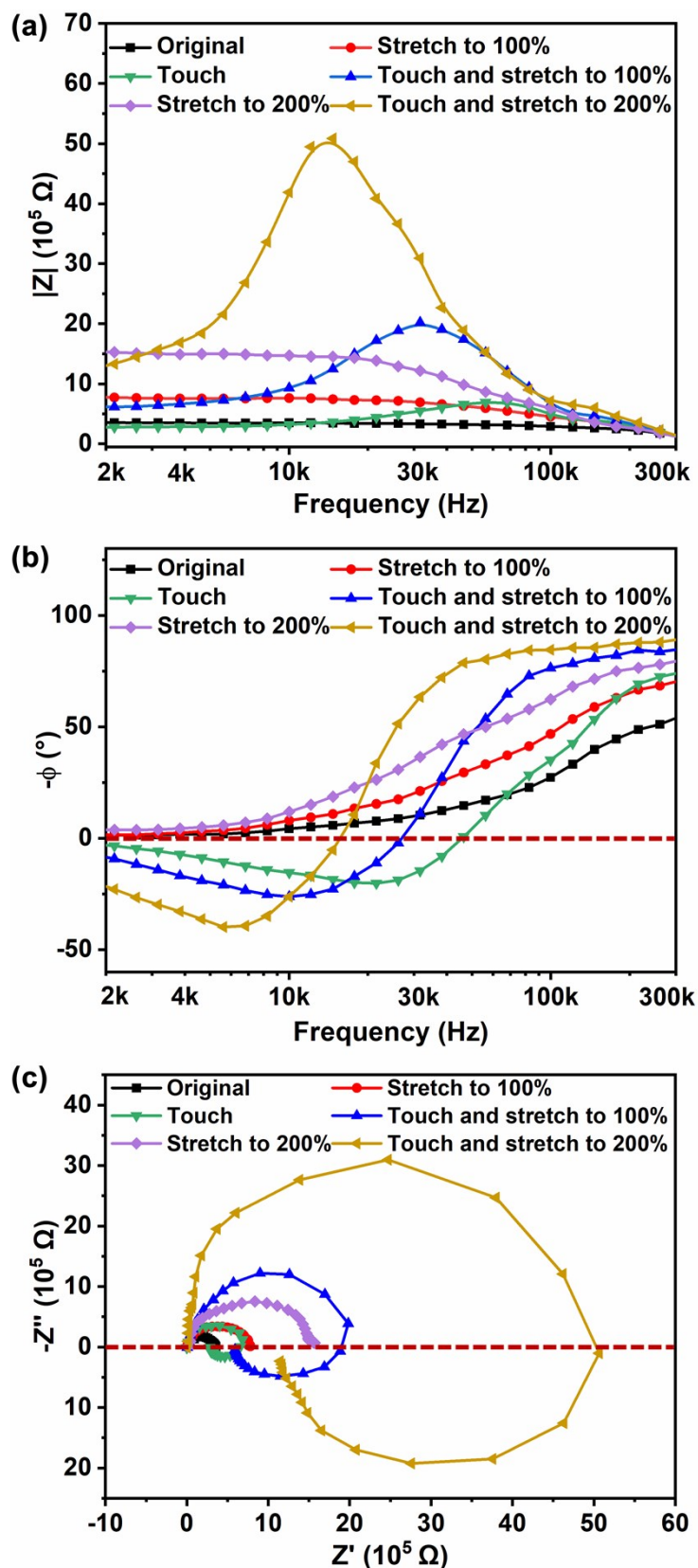


Fig. S12 (a-c) $|Z|$ - f (a), $-\phi$ - f (b), $-Z''$ - Z' (c) plots (i.e., electrochemical impedance spectra) of the AC circuit, collected when the PIL-2/TFSI elastomer was subjected to different stimuli.

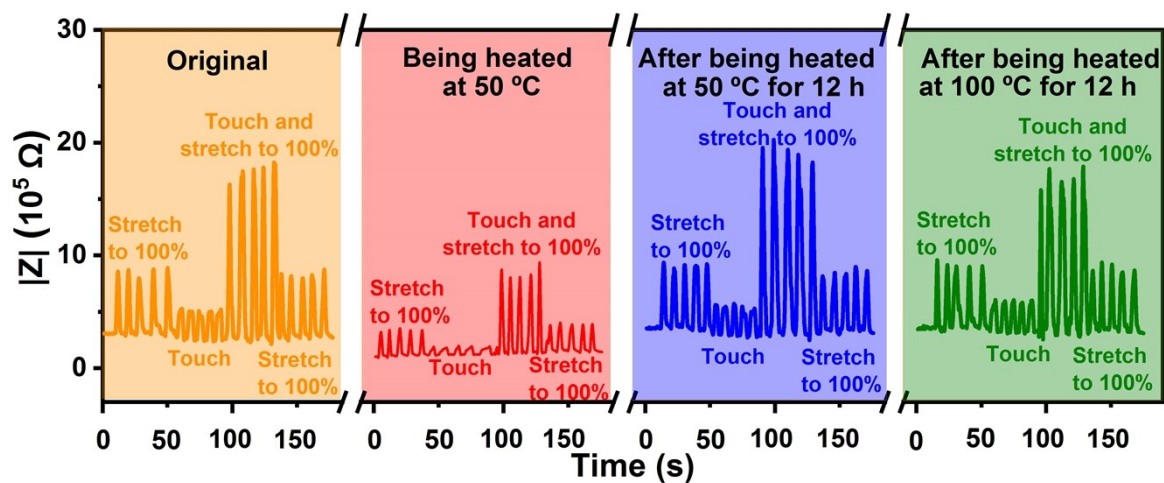


Fig. S13 Real-time response of $|Z|$ of the stretchable touch sensor to the repeated different stimuli, including stretch, touch and touch on the basis of stretch when or after the PIL-2/TFSI elastomer was subjected to different operations.